Angewandte Chemie
Eine Zeitschrift der Gesellschaft Deutscher Chemiker

Supporting Information

How Crystal Symmetry Dictates Non-Local Vibrational Circular Dichroism in the Solid State

S. Jähnigen, K. Le Barbu-Debus, R. Guillot, R. Vuilleumier, A. Zehnacker**

Supporting Information: How Crystal Symmetry Dictates Non-Local Vibrational Circular Dichroism in the Solid State

Sascha Jähnigen,*,† Katia Le Barbu-Debus,‡ Régis Guillot,¶ Rodolphe Vuilleumier,† and Anne Zehnacker*,‡

†*PASTEUR, Département de Chimie, Ecole Normale Supérieure, PSL University, Sorbonne Université, CNRS, 75005 Paris, France*

‡*Institut des Sciences Moléculaires d'Orsay (ISMO), CNRS, Université Paris-Saclay, 91405 Orsay, France*

¶*Institut de Chimie Moléculaire et des Matériaux d'Orsay (ICMMO), CNRS, Université Paris-Saclay, 91405 Orsay, France*

E-mail: sascha.jahnigen@ens.psl.eu; anne.zehnacker-rentien@universite-paris-saclay.fr

Experimental Methods

Crystallography

X-ray diffraction data was collected by using a VENTURE PHOTON100 CMOS Bruker diffractometer with Microfocus IuS source Cu Kα radiation. The crystal sample was mounted on a CryoLoop (Hampton Research) with Paratone-N (Hampton Research) as cryoprotectant and then flash frozen in a nitrogen-gas stream at 250 K. The temperature of the crystal was

Table S1: Crystallographic data for (*S*)-(+)-1-indanol (CCDC 2077885).[S5] Cell lengths a, b, c (Å), cell angles α, β, γ (°), cell volume V (Å^3). The data has been recorded at 250 K. Z and Z' are the number of molecules in the unit cell and in the asymmetric unit, respectively.

Compound	(*S*)-(+)-1-indanol
Crystal system	monoclinic
Space group	$P\,2_1$
a	6.9817(9)
b	4.8408(6)
c	10.9052(14)
α	90
β	95.563(5)
γ	90
V	366.83(8)
Z; Z'	2; 1

maintained at the selected value (250K) by means of a 700+ series Cryostream cooling device to within an accuracy of ±1 K. The data was corrected for Lorentz polarization and absorption effects. The structures were solved by direct methods using SHELXS-97[S1] and refined against F2 by full-matrix least-squares techniques using SHELXL-2018[S2] with anisotropic displacement parameters for all non-hydrogen atoms. Hydrogen atoms were located on a difference Fourier map and introduced into the calculations as a riding model with isotropic thermal parameters. All calculations were performed with the Crystal Structure crystallographic software package WINGX.[S3] The crystal data collection and refinement parameters are given in Table S1. The absolute configuration was determined for (*S*)-(+)-1-indanol by refining the Flack's parameter[S4] using a large number of Friedel's pairs.

Experimental Spectroscopy

The vibrational infrared (IR) absorption and VCD spectra of the enantiopure forms of solid (*S*)-(+)-1-indanol were measured using a Fourier-transform infrared spectroscopy (FTIR) spectrometer (Vertex 70, Bruker) equipped with a VCD module (PMA 50, Bruker), as previously described.[S6–S9] The filtered and linearly polarized IR radiation was modulated by

a 50 kHz ZnSe photo-elastic modulator (Hinds). The signal was measured by a Mercury-Cadmium-Telluride (MCT) IR detector and demodulated by a lock-in amplifier (Stanford Research Systems SR 830), with a spectral resolution of 4 cm^{-1} and a total measurement time of 4h. The alignment of the spectrometer was controlled by checking the mirror-image relation between the VCD spectra of the two enantiomers of camphor (0.3 M in CCl_4). The samples were prepared by grinding 10 mg of 1-indanol with 1 g of KBr in a mixer mill (MM 400 Retsch) at 20 Hz during 30 min and pressing 150 to 200 mg pellets. Linear dichroism artefacts were eliminated following the procedure reported in the literature.[S10,S11] It consists in averaging the spectra obtained for the pellets rotated at 0° and 90° in the plane perpendicular to the light propagation axis for each side of the pellet. When not specified otherwise, the VCD spectrum discussed in this paper is the half difference of the VCD spectra of the S and R enantiomers of 1-indanol.

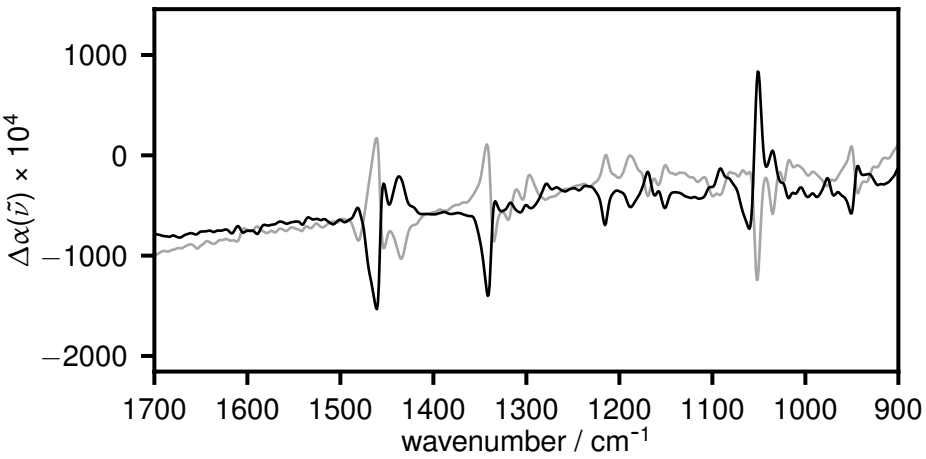

Figure S1: Experimental VCD spectra of (*S*)-(+)-1-indanol (black) and (*R*)-(−)-1-indanol (grey) obtained in solid-state from a KBr pellet.

Computational Details

Dynamic Calculations on the Bulk Crystal with AIMD

A 2×2×1 supercell of crystalline (*S*)-(+)-1-indanol was considered based on the obtained crystal structure (*cf.* Table S1). The system was optimised an pre-equilibrated for 50 ps using CP2K 6.1[S12] and AmberTools20[S13] with the GAFF2 force field.[S13] Then, Born-Oppenheimer AIMD simulations were carried out with the CP2K 5.1[S12] program package via the Quickstep module,[S14] describing the exchange-correlation energy with the GGA functional BLYP for equilibration (3.5 ps) and the hybrid functional B3LYP for production (27 ps),[S15–S20] the DZVP-MOLOPT-SR-GTH basis set,[S21] the cFIT3 auxiliary basis for ADMM[S22] using a cutoff radius of 4.95 Å[S23] and GTH pseudo-potentials[S24–S26] with a 0.5 fs time step, a density cutoff of 400 Ry, and Grimme's dispersion correction (D3).[S27] The CSVR[S28] thermostat was used at 320 K (coupling constant: equilibration 10-100 fs with massive and global thermostatting; production 1000 fs with global thermostatting).

Projected NVPT calculations were carried out with CPMD 4.3[S29–S31] sampling over the previously created FPMD trajectory, using the BLYP functional, a plane wave basis with a cutoff of 100 Ry, Troullier–Martins pseudo potentials[S32] and the Kleinman-Bylander separation scheme.[S33] The trajectory was sampled at every eighth step to form the correlation function, resulting in a time resolution of 4 fs for current and magnetic dipole moments.

The computation of IR and VCD spectra was carried out in the Heisenberg representation using the the Fourier transform of the time-correlation function (FT-TCF) and the newly described gauge for the magnetic dipole moment, as implemented in the python package *ChirPy* 0.23.2, available on GitLab.[S34] See also the provided Jupyter notebook for further details (`https://doi.org/10.5281/zenodo.7228748`). Effective normal modes were extracted using *ChirPy* 0.23.0.

Peak alignment was done using the IRSA algorithm originally developed by Riniker and co-workers[S35] and extended to continuous spectra by our group,[S36] using same parameters

as in the reference for the scoring function ($\sigma_I = 0.25$, $\sigma_{\tilde{\nu}} = 0.025$, $\mu_I = 1.0$, $\mu_{\tilde{\nu}} = 1.0$; cutoff 0.0 a.u. and 40 cm^{-1} for intensities I and wavenumbers $\tilde{\nu}$, respectively). Figures S2, S3, and S4 shows the data preparation and the resulting frequency shifts in analogy to the reference.[S36]

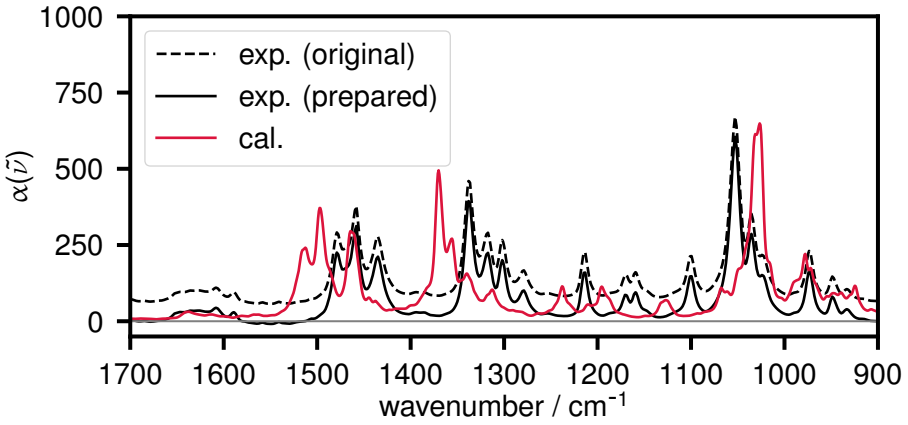

Figure S2: Preparation of the experimental IR spectrum for the IRSA algorithm.

S36

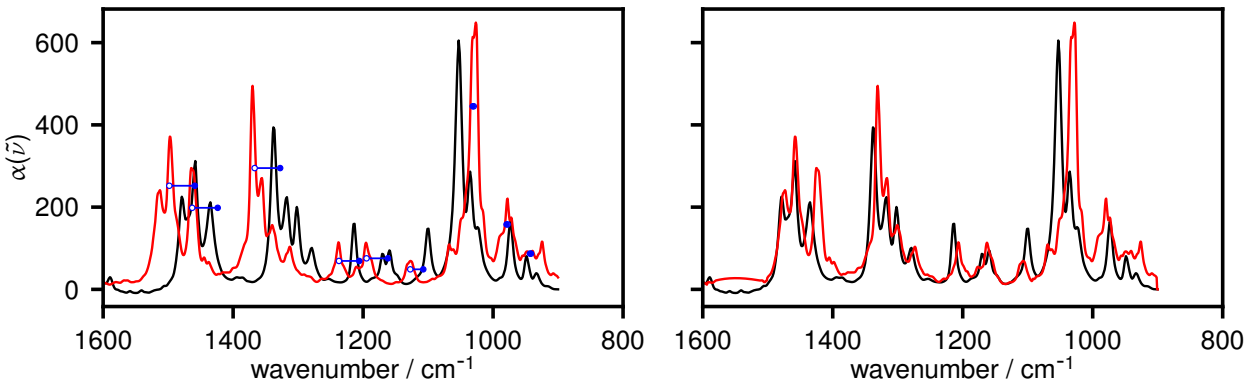

Figure S3: Changed peak position of the calculated spectrum (red) after application of the IRSA algorithm, compared to the experimental spectrum (black). Left: before. Right: after. The alignment did not succeed for the CC/CO stretching band due to the different intensity distribution of the band.

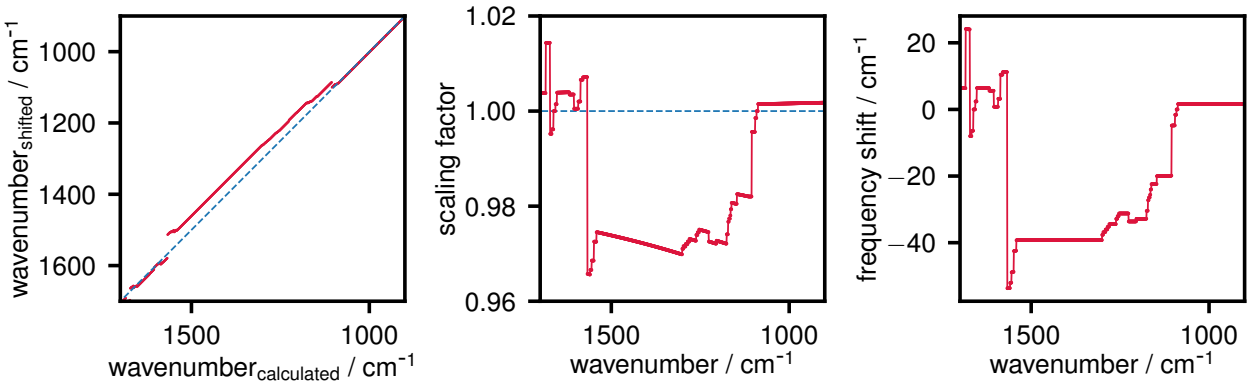

Figure S4: Frequency shift alignment with the IRSA algorithm. Left: Scatter plot of original and shifted frequencies. Center: Resulting frequency-dependent scaling factor. Right: Absolute shift in frequency.

Static Calculations on a Cluster Model using the Hessian Matrix

The solid-state structure of (*S*)-(+)-1-indanol was first optimised in the frame of the density functional theory (DFT) using periodic boundary conditions (PBC), with the B3LYP functional and the 6-31G(d,p) basis set.[S16–S19,S37] The experimental crystal geometry was used as an input. Then, sub-units of increasing size were extracted from the PBC results and optimised in the frame of the density functional theory (DFT) using the B3LYP functional including D3BJ corrections and the 6-311++G(d,p) basis set.[S37,S38] The frequencies were calculated at the same level of theory in the double harmonic approximation. The harmonic frequencies were scaled by 0.975 to account for anharmonicity and basis set incompleteness.[S39] The values mentioned in the text are the scaled frequencies. All calculations were performed using version G16 Revision B.01 of the Gaussian software.[S40]

Other

Plots were generated with python-based Matplotlib 3.0.1.[S41] Molecular visualisations were created with VMD 1.9.3[S42] using the Tachyon Ray Tracer.[S43] All figures were post-processed with Gimp 2.10.18.[S44]

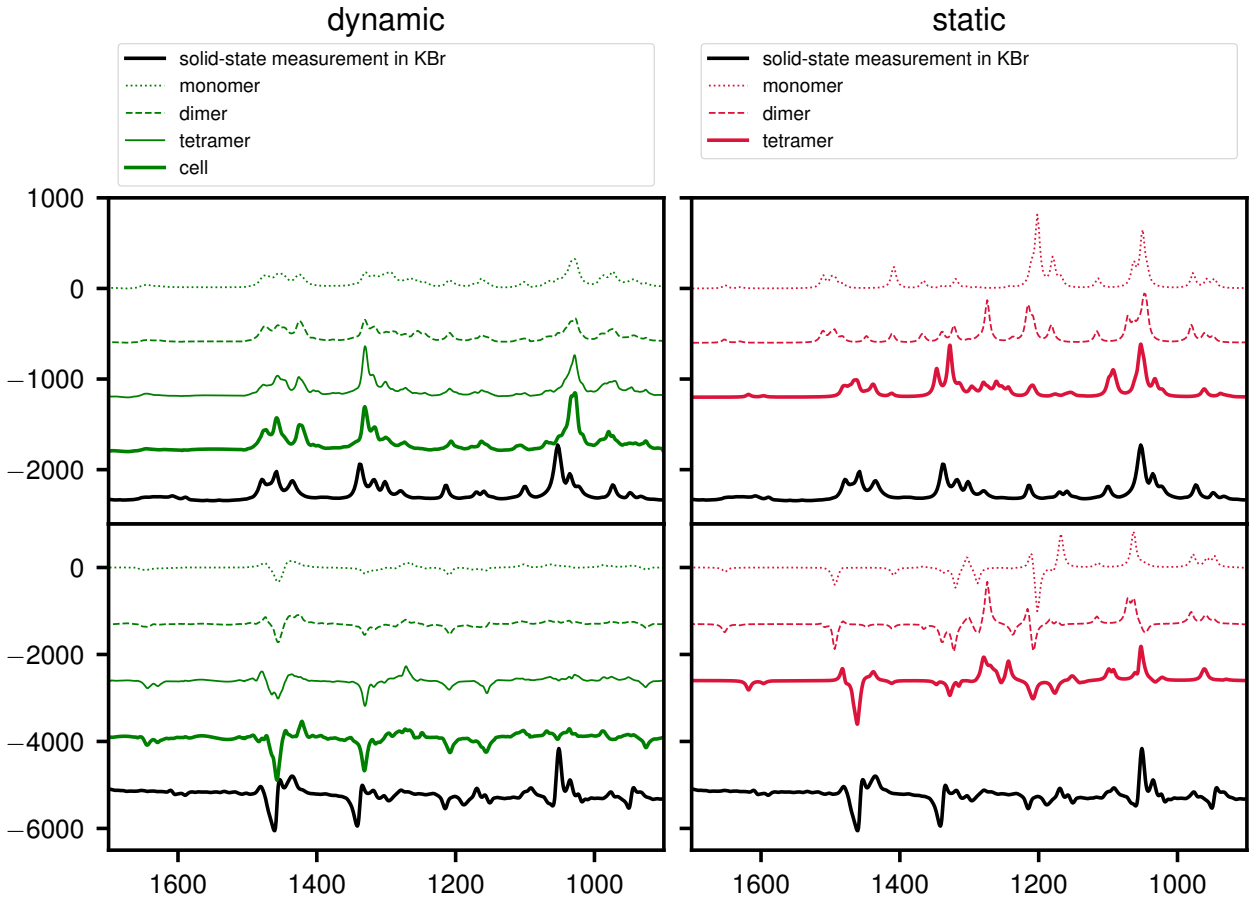

Figure S5: Computed IR absorption and VCD spectra for cluster models of increasing size (left: extracted from the AIMD-NVPT trajectory; right: individual calculations, see Computational Methods).

Table S2: Experimental wavenumbers of the most important observed bands measured in KBr and assignment based on normal modes from static and dynamic calculations (see above). Many vibrations include the aromatic system; the given symmetry descriptors do not denote the actual symmetry of the vibration, but facilitate the assignment with reference to benzene (D_{6h}). For artefacts of the static calculations, the scaled wavenumbers are written as they appear in Figure 3.

Wavenumbers[a]	VCD sign	Assignment
932–947	−/+	ν(C_2–C_3)
970	+	ν_{as}(C_2–C_3/C_1–C_2)
1023	+	$\nu_{ar}(a_{1g})$ (“breathing”)
1036	+	ν(C_1–C_2)
1054	+	ν_{as}(C_1–O/C_1–C_2)
1100	+	ν(C_1–O)
1160/ 1170	+/−	aromatic/aliphatic δ(C–H) combinations
1214	−	$\nu_{ar}(a_{1g})$ (“breathing”) + ν_s(C_1–C_9/C_3–C_4)
1280	+	$\delta_{ar}(a_{2g})$ + ρ(C–H_{ax})
1300	+	$\delta_{ar}(a_{2g})$ + δ_{wag}(CH_2)
1317	+	$\nu_{ar}(b_{2u})$ + δ_{as}(O–H/C_1–H) (“anti-parallel windshield wiper”)
1340	−/+	$\nu_{ar}(b_{2u})$ + ρ(C_1–H)
1434	+	δ_s(O–H/C_1–H) (“parallel windshield wiper”) + δ(C_{ar}–H)
1460	−	$\nu/\delta^1_{ar}(e_{1u})$ + δ_{sciss}(CH_2)
1478	+	$\nu/\delta^2_{ar}(e_{1u})$ + δ_{sciss}(CH_2)
Artefacts:		
1248	+	dangling “anti-parallel windshield wiper”
1268	+	wrong frequencies and intensities due to unsatisfactory description of the coupling between the molecules; mainly $\delta_{wag/twist}$(CH_2) and ρ(C_1–H)
1286	+	
1334	−	
1418	−	dangling “parallel windshield wiper’

[a] in cm^{-1}

Symmetry and Directionality of Non-Local VCD Terms

The definition of VCD for a system of multiple sub-units to be defined are given as Equations 1 and 2 in the main text. Hence, for a vibrational transition a the rotational strength R^a is calculated from the current and magnetic dipole moment, j^a and m^a, bound to this transition,

$$R^a = \mathrm{j}^a \otimes \mathrm{m}^a \tag{1}$$

$$= \underbrace{\sum_k \mathrm{j}_k^a \otimes \mathrm{m}_k^a}_{\text{local}} + \underbrace{\sum_k \sum_{l \neq k} \mathrm{j}_k^a \otimes \mathrm{m}_l^a}_{\text{non-local}}, \tag{2}$$

wherefrom the local and non-local terms can immediately be selected. Here we introduce a general $\otimes$ notation, valid for the static and the dynamic formalism alike, because this derivation can be done in either representation without loss of generality. Hence, the rotational strength can either be calculated from the transition dipole moments of mode a (static) or from the spectral density expressed as the Fourier-transform of the time-correlation function, at vibrational frequency ω_a (dynamic):[S36]

$$\mathrm{j}_k^a \otimes \mathrm{m}_l^a = \mathrm{j}_k^a \cdot \mathrm{m}_l^a \tag{3}$$

$$= \mathcal{F}\big[\langle \mathrm{j}_k(0)\mathrm{m}_l(t)\rangle\big](\omega_a). \tag{4}$$

Invoking the gauge dependence of the magnetic dipole moment (*cf.*, Equation 3 in the main text), the non-local VCD terms can be distinguished as direct coupling (DC) and gauge transport (GT) terms,

$$\mathrm{j}_k^a \otimes \mathrm{m}_l^a = \mathrm{j}_k^a \otimes \left(\mathrm{m}_l^{a,\mathrm{local}} + \frac{1}{2c}\mathrm{r}_l \times \mathrm{j}_l^a\right) = \underbrace{\mathrm{j}_k^a \otimes \mathrm{m}_l^{a,\mathrm{local}}}_{DC} + \underbrace{\frac{1}{2c}\mathrm{j}_k^a \otimes \left(\mathrm{r}_l \times \mathrm{j}_l^a\right)}_{GT}, \tag{5}$$

where displacement vector r_l denotes the relative position of the units according to the nearest image convention[S36] and $\mathrm{m}_l^{a,\mathrm{local}}$ the intrinsic magnetic moment of the unit.

In solid state, a natural choice for the smallest unit is the asymmetric unit of the crystal, which is, in the case of Sohncke space groups, mostly a single molecule. The molecular units are then related to each other by the symmetry of the crystal, which determines non-local VCD.

Here, we focus on the $\mathrm{P2_1}$ space group and notice *a priori* that for the generation of non-local VCD, twofold rotary translation is equivalent to simple twofold rotation, because a displacement along the screw axis has no effect on VCD for neither DC nor GT terms. The former because it does not depend on the relative position of the units (but their relative orientation), the latter because rotation by π renders the dipole vectors and the parallel displacement vector in the same plane and thus a vanishing triple product in Equation 5.

Hence, the $\hat{2}_1$ operation reduces to a simple $\hat{2}$ rotation, which reads in Cartesian coordinates:

$$\hat{2} = \begin{pmatrix} -1 & 0 & 0 \\ 0 & 1 & 0 \\ 0 & 0 & -1 \end{pmatrix}. \tag{6}$$

The current and magnetic dipole moments, as well as the position vector are written as $\mathrm{j} = (j_x, j_y, j_z)^{\mathrm{T}}$, $\mathrm{m} = (m_x, m_y, m_z)^{\mathrm{T}}$, and $\mathrm{r} = (r_x, r_y, r_z)^{\mathrm{T}}$, respectively; application of $\hat{2}$ gives:

$$\hat{2} \begin{pmatrix} j_x \\ j_y \\ j_z \end{pmatrix} = \begin{pmatrix} -j_x \\ j_y \\ -j_z \end{pmatrix}, \tag{7}$$

likewise for m and r.

In $\mathrm{P2_1}$, the unit cell contains only two units and Equation 2 simplifies to

$$R^a = \underbrace{(\mathrm{j}_1^a \otimes \mathrm{m}_1^a \; + \; \mathrm{j}_2^a \otimes \mathrm{m}_2^a)}_{\text{local}} + \underbrace{(\mathrm{j}_1^a \otimes \mathrm{m}_2^a \; + \; \mathrm{j}_2^a \otimes \mathrm{m}_1^a)}_{\text{non-local}}. \tag{8}$$

The (asymmetric) units are related via the space group's symmetry operations $\hat{A}$ and a mode phase factor $p = \cos\phi$, so that $\mathrm{j}_2 = p\,\hat{A}\mathrm{j}_1$ *etc.* It follows:

$$R^a = \underbrace{\left(\mathrm{j}_1^a \otimes \mathrm{m}_1^a \;+\; p\,\hat{A}\mathrm{j}_1 \otimes p\,\hat{A}\mathrm{m}_1\right)}_{\text{local}} + \underbrace{\left(\mathrm{j}_1^a \otimes p\,\hat{A}\mathrm{m}_1 \;+\; p\,\hat{A}\mathrm{j}_1 \otimes \mathrm{m}_1^a\right)}_{\text{non-local}}. \tag{9}$$

Now index 1 can be dropped and after division by the number of units ($N = 2$), the rotational strength per mole reads:

$$R_m^a = \underbrace{\frac{1+p^2}{N}\mathrm{j}^a \otimes \mathrm{m}^a}_{\text{local}} + \frac{2p}{N}\underbrace{\left(\hat{A}\mathrm{j}^a \otimes \mathrm{m}^a\right)}_{\text{non-local}} \tag{10}$$

$$R_m^a = \underbrace{\frac{1+p^2}{N}\mathrm{j}^a \otimes \mathrm{m}^{a,\mathrm{local}}}_{\text{local}} + \frac{2p}{N}\underbrace{\left(\hat{A}\mathrm{j}^a \otimes \mathrm{m}^{a,\mathrm{local}}\right)}_{\text{DC}} + \frac{p}{cN}\underbrace{\left(\hat{A}\mathrm{j}^a \otimes \left(\mathrm{r} \times \mathrm{j}^a\right)\right)}_{\text{GT}}. \tag{11}$$

where we acknowledge that $\otimes$ is invariant under $\hat{A}$ and that all symmetry operations in $P2_1$ are self-inverse, $\hat{A} = \hat{A}^{-1}$, modulo a lattice translation $\hat{T}$. It has to be noted that in $P2_1$ with only two units, the phase factor p can only take the values $+1$ or -1 corresponding to in-phase or out-of-phase vibrations, while beyond that, only $k = 0$ phonons contribute to IR absorption and VCD.

If $\hat{A}$ is the translation operation $\hat{T}$, all GT terms vanish and Equation 11 simplifies to

$$R_m^{a,\hat{T}} = \frac{(1+p)^2}{N}\mathrm{j}^a \otimes \mathrm{m}^{a,\mathrm{local}}, \tag{12}$$

that is, translation can only increase or decrease local VCD as a whole depending on the vibrational mode phase between molecules. This is in agreement with Figure 3 (center) in the main text.

For rotation, in turn, where $\hat{A} = \hat{2}$ (corresponding to $\hat{2}_1$; see above), new non-local VCD

peaks emerge from

$$R_m^{a,\hat{2}} = \underbrace{\frac{1+p^2}{N}\mathrm{j}^a \otimes \mathrm{m}^{a,\mathrm{local}}}_{\text{local}} + \frac{2p}{N}\underbrace{\left(\hat{2}\mathrm{j}^a \otimes \mathrm{m}^{a,\mathrm{local}}\right)}_{\text{DC}} + \frac{p}{cN}\underbrace{\left(\hat{2}\mathrm{j}^a \otimes \left(\mathrm{r} \times \mathrm{j}^a\right)\right)}_{\text{GT}}. \tag{13}$$

First, the DC term is rendered with a directionality that interferes with the local term:

$$\begin{aligned} R_m^{a,\hat{2},\mathrm{local+DC}} &= \frac{1+p^2}{N}\mathrm{j}^a \otimes \mathrm{m}^a \; + \; \frac{2p}{N}\hat{2}\mathrm{j}^a \otimes \mathrm{m}^a & (14)\\ &= \frac{2}{N}\left(j_x^a m_x^a + j_y^a m_y^a + j_z^a m_z^a\right) \; + \; \frac{2p}{N}\left(-j_x^a m_x^a + j_y^a m_y^a - j_z^a m_z^a\right) & (15)\\ &= \frac{2}{N}\left[\underbrace{(1-p)\left(j_x^a m_x^a + j_z^a m_z^a\right)}_{\text{orthogonal}} + \underbrace{(1+p)\, j_y^a m_y^a}_{\text{parallel}}\right], & (16) \end{aligned}$$

where we dropped the superscript "local" for clarity. Consequently, depending on the phase, -1 or $+1$, of the delocalised vibrational mode, the VCD-effective polarisation can be found as either orthogonal or parallel to the screw axis, but not as both at the same time. This symmetry-selective quenching and enhancement has the capacity to give rise to entirely new VCD peaks that are absent locally, like it is showcased in Scheme 2 and obtained for (*S*)-(+)-1-indanol at 1434 cm^{-1} (*cf.*, Figures 3, S6, S7).

Second, the GT term,

$$\begin{aligned} R_m^{a,\hat{2},\mathrm{GT}} &= \frac{p}{cN}\hat{2}\mathrm{j}^a \otimes \left(\mathrm{r} \times \mathrm{j}^a\right). & (17)\\ &= \frac{p}{cN}\det\left[\,\hat{2}\mathrm{j}^a \quad \mathrm{r} \quad \mathrm{j}^a\,\right], & (18) \end{aligned}$$

can be interpreted best by looking at the determinant's properties:

$$\det\left[\,\hat{2}\mathrm{j}^a \quad \mathrm{r} \quad \mathrm{j}^a\,\right] = \begin{bmatrix} -j_x^a & r_x & j_x^a \\ j_y^a & r_y & j_y^a \\ -j_z^a & r_z & j_z^a \end{bmatrix} \tag{19}$$

A determinant vanishes if two rows are equal or linear dependent. Here, this is the case when

r_x and r_z are zero, that is, when r is parallel to the screw axis. This is why the correspondence $\hat{2}_1 \rightarrow \hat{2}$ is valid for the GT term, too. It also follows that r has to be orthogonal to j^a. Furthermore and most importantly, both, orthogonal (x and z) and parallel (y) polarisation of j^a must be non-zero, as both parts contribute to the product. This stands in contrast to the DC term, where either orthogonal or parallel polarisation is favoured. These conditions are fulfilled in crystals of (S)-(+)-1-indanol for certain peaks, most prominently in the region 1400–1455 cm^{-1} (Figure 3), but also in other regions of the spectrum (Figure S6). The sightedness of the GT term in $P2_1$ can readily be determined, which amounts to $2\sqrt{r_x^2 + r_z^2}$, that is, approximately 5 Å for (S)-(+)-1-indanol.

In order to provide with this derivation a concrete example, the vibrational mode at 1435 cm^{-1} is depicted in Figure S7.

A similar derivation can be made for IR absorption, which, however, only involves the direct term given that it fully relies on polar vectors.

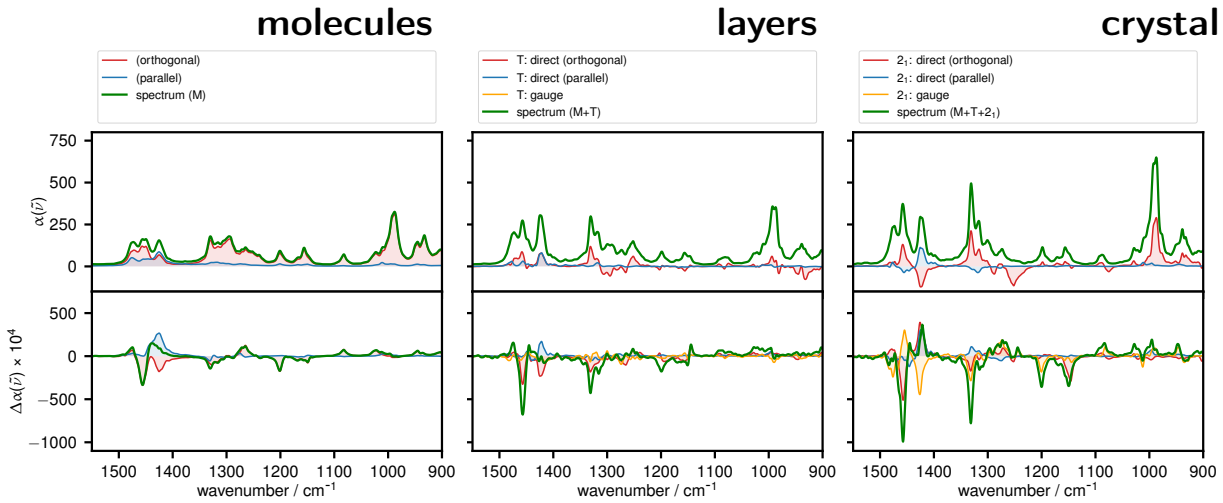

Figure S6: The emergence of non-local VCD in $P2_1$ crystals of (S)-(+)-1-indanol, full spectrum (*cf.*, Figure 3 in the main text). IR absorption and VCD (sub-)spectra from AIMD-NVPT calculations. Direct coupling is shown in red and blue for parallel and orthogonal polarisation, respectively; gauge transport in yellow (full spectrum shown in green). M: Molecule; T: Translation; 2_1: Twofold screw axis.

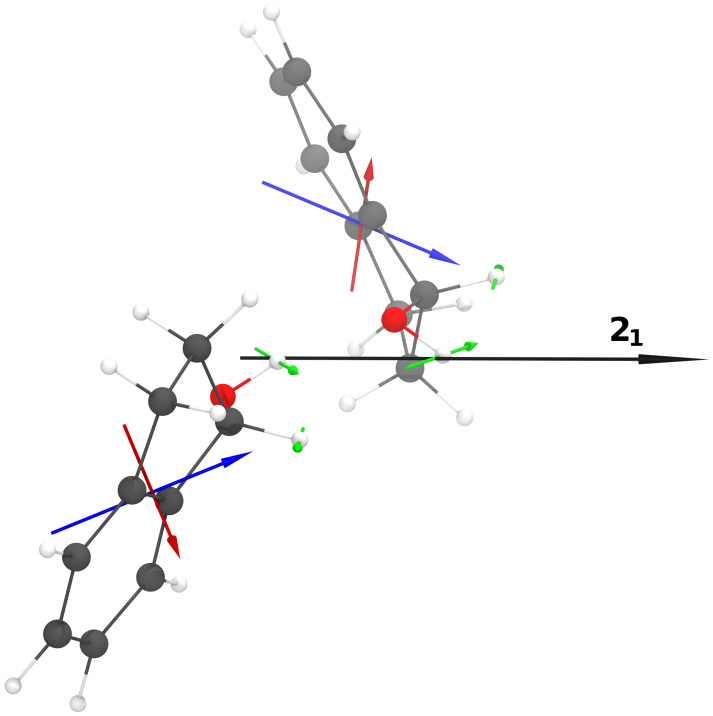

Figure S7: Effect of crystal symmetry on vibrational polarisation at the example of the "parallel windshield wiper" mode at 1434 cm^{-1}. Green arrows: delocalised normal mode a; black arrow: twofold screw axis; blue arrows: current transition dipole moment, j^a; red arrows: magnetic transition dipole moment, m^a. The non-local VCD terms emerging from this arrangement, according to Equations 16 and 18, correspond to Scheme 2, yielding positive VCD via DC and negative VCD via GT ($p = 1$).

References

(S1) Sheldrick, G. M. SHELXS-97, Program for Crystal Structure Solution. University of Göttingen, 1997.

(S2) Sheldrick, G. M. SHELXL-97, Program for the Refinement of Crystal Structures from Diffraction Data. University of Göttingen, 1997.

(S3) Farrugia, L. J. WinGX Suite for Small-Molecule Single-Crystal Crystallography. *J. Appl. Crystallogr.* **1999**, *32*, 837–838.

(S4) Flack, H. D. On Enantiomorph-Polarity Estimation. *Acta Crystallogr. Sect. A* **1983**, *39*, 876–881.

(S5) Deposition Number 2077885 contains the supplementary crystallographic data for this paper. These data are provided free of charge by the joint Cambridge Crystallographic Data Centre and Fachinformationszentrum Karlsruhe Access Structures service www.ccdc.cam.ac.uk/structures.

.

(S6) Pérez-Mellor, A.; Zehnacker, A. Vibrational Circular Dichroism of a 2,5-Diketopiperazine (DKP) Peptide: Evidence for Dimer Formation in Cyclo LL or LD Diphenylalanine in the Solid State. *Chirality* **2017**, *29*, 89–96.

(S7) Pérez-Mellor, A.; Barbu-Debus, K. L.; Zehnacker, A. Solid-State Synthesis of Cyclo LD-diphenylalanine: A Chiral Phase Built from Achiral Subunits. *Chirality* **2020**, *32*, 693–703.

(S8) Li, X.; Porcino, M.; Martineau-Corcos, C.; Guo, T.; Xiong, T.; Zhu, W.; Patriarche, G.; Péchoux, C.; Perronne, B.; Hassan, A.; Kümmerle, R.; Michelet, A.; Zehnacker-Rentien, A.; Zhang, J.; Gref, R. Efficient Incorporation and Protection of Lansoprazole in Cyclodextrin Metal-Organic Frameworks. *International Journal of Pharmaceutics* **2020**, *585*, 119442.

(S9) Sen, A.; Bouchet, A.; Lepère, V.; Le Barbu-Debus, K.; Scuderi, D.; Piuzzi, F.; Zehnacker-Rentien, A. Conformational Analysis of Quinine and Its Pseudo Enantiomer Quinidine: A Combined Jet-Cooled Spectroscopy and Vibrational Circular Dichroism Study. *J. Phys. Chem. A* **2012**, *116*, 8334–8344.

(S10) Merten, C.; Kowalik, T.; Hartwig, A. Vibrational Circular Dichroism Spectroscopy of Solid Polymer Films: Effects of Sample Orientation. *Appl Spectrosc* **2008**, *62*, 901–905.

(S11) Buffeteau, T.; Lagugné-Labarthet, F.; Sourisseau, C. Vibrational Circular Dichroism

in General Anisotropic Thin Solid Films: Measurement and Theoretical Approach. *Appl. Spectrosc., AS* **2005**, *59*, 732–745.

(S12) The CP2K Developers Group, 2001–2021. `https://www.cp2k.org`.

(S13) Case, D. A.; Aktulga, H. M.; Belfon, K.; Ben-Shalom, I. Y.and Brozell, S. R.; Cerutti, D. S.; Cheatham, T. E.; Cruzeiro, V. W. D.; Darden, T. A.; Duke, R. E.; Giambasu, G.; Gilson, M. K.; Gohlke, H.; Goetz, A. W.; Harris, R.; Izadi, S.; Izmailov, S. A.; Jin, C.; Kasavajhala, K.; Kaymak, M. C.; King, E.; Kovalenko, A.; Kurtzman, T.; Lee, T. S.; LeGrand, S.; Li, P.; Lin, C.; Liu, J.; Luchko, T.; Luo, R.; Machado, M.; Man, V.; Manathunga, M.; Merz, K. M.; Miao, Y.; Mikhailovskii, O.; Monard, G.; Nguyen, H.; O'Hearn, K. A.; Onufriev, A.; Pan, F.; Pantano, S.; Qi, R.; Rahnamoun, A.; Roe, D. R.; Roitberg, A.; Sagui, C.; Schott-Verdugo, S.and Shen, J.; Simmerling, C. L.; Skrynnikov, N. R.; Smith, J.; Swails, J.; Walker, R. C.; Wang, J.; Wei, H.; Wolf, R. M.; Wu, X.; Xue, Y.; York, D. M.; Zhao, S.; Kollman, P. A. Amber20. University of California, San Francisco, 2020; `www.ambermd.org`.

(S14) VandeVondele, J.; Krack, M.; Mohamed, F.; Parrinello, M.; Chassaing, T.; Hutter, J. QUICKSTEP: Fast and Accurate Density Functional Calculations Using a Mixed Gaussian and Plane Waves Approach. *Comput. Phys. Commun.* **2005**, *167*, 103–128.

(S15) Stephens, P. J.; Devlin, F. J.; Chabalowski, C. F.; Frisch, M. J. Ab Initio Calculation of Vibrational Absorption and Circular Dichroism Spectra Using Density Functional Force Fields. *J. Phys. Chem.* **1994**, *98*, 11623–11627.

(S16) Becke, A. D. Density-functional Thermochemistry. III. The Role of Exact Exchange. *The Journal of Chemical Physics* **1993**, *98*, 5648–5652.

(S17) Becke, A. D. Density-Functional Exchange-Energy Approximation with Correct Asymptotic Behavior. *Phys. Rev. A* **1988**, *38*, 3098–3100.

(S18) Lee, C.; Yang, W.; Parr, R. G. Development of the Colle-Salvetti Correlation-Energy Formula into a Functional of the Electron Density. *Phys. Rev. B* **1988**, *37*, 785–789.

(S19) Vosko, S. H.; Wilk, L.; Nusair, M. Accurate Spin-Dependent Electron Liquid Correlation Energies for Local Spin Density Calculations: A Critical Analysis. *Can. J. Phys.* **1980**, *58*, 1200–1211.

(S20) Guidon, M.; Schiffmann, F.; Hutter, J.; VandeVondele, J. *Ab Initio* Molecular Dynamics Using Hybrid Density Functionals. *The Journal of Chemical Physics* **2008**, *128*, 214104.

(S21) VandeVondele, J.; Hutter, J. Gaussian Basis Sets for Accurate Calculations on Molecular Systems in Gas and Condensed Phases. *J. Chem. Phys.* **2007**, *127*, 114105.

(S22) Guidon, M.; Hutter, J.; VandeVondele, J. Auxiliary Density Matrix Methods for Hartree-Fock Exchange Calculations. *J. Chem. Theory Comput.* **2010**, *6*, 2348–2364.

(S23) Guidon, M.; Hutter, J.; VandeVondele, J. Robust Periodic Hartree-Fock Exchange for Large-Scale Simulations Using Gaussian Basis Sets. *J. Chem. Theory Comput.* **2009**, *5*, 3010–3021.

(S24) Goedecker, S.; Teter, M.; Hutter, J. Separable Dual-Space Gaussian Pseudopotentials. *Phys. Rev. B* **1996**, *54*, 1703–1710.

(S25) Hartwigsen, C.; Goedecker, S.; Hutter, J. Relativistic Separable Dual-Space Gaussian Pseudopotentials from H to Rn. *Phys. Rev. B* **1998**, *58*, 3641–3662.

(S26) Krack, M. Pseudopotentials for H to Kr Optimized for Gradient-Corrected Exchange-Correlation Functionals. *Theor. Chem. Acc.* **2005**, *114*, 145–152.

(S27) Grimme, S.; Antony, J.; Ehrlich, S.; Krieg, H. A Consistent and Accurate Ab Initio Parametrization of Density Functional Dispersion Correction (DFT-D) for the 94 Elements H-Pu. *J. Chem. Phys.* **2010**, *132*, 154104.

(S28) Bussi, G.; Donadio, D.; Parrinello, M. Canonical Sampling through Velocity Rescaling. *J. Chem. Phys.* **2007**, *126*, 014101.

(S29) Scherrer, A.; Vuilleumier, R.; Sebastiani, D. Nuclear Velocity Perturbation Theory of Vibrational Circular Dichroism. *J. Chem. Theory Comput.* **2013**, *9*, 5305–5312.

(S30) Scherrer, A.; Vuilleumier, R.; Sebastiani, D. Vibrational Circular Dichroism from Ab Initio Molecular Dynamics and Nuclear Velocity Perturbation Theory in the Liquid Phase. *J. Chem. Phys.* **2016**, *145*, 084101.

(S31) CPMD 4.1.0, Copyright 2000–2019. IBM Corp. and by Max Planck Institute, Stuttgart, `https://www.cpmd.org`.

(S32) Troullier, N.; Martins, J. L. Efficient Pseudopotentials for Plane-Wave Calculations. *Phys. Rev. B* **1991**, *43*, 1993–2006.

(S33) Kleinman, L.; Bylander, D. M. Efficacious Form for Model Pseudopotentials. *Phys. Rev. Lett.* **1982**, *48*, 1425–1428.

(S34) Jähnigen, S. *ChirPy – A Python Package for Chirality Dynamics, and Molecular Vibrations*, Ver. 0.23.2; Zenodo, 2022; `http://doi.org/10.5281/zenodo.4775330`.

(S35) Böselt, L.; Dötzer, R.; Steiner, S.; Stritzinger, M.; Salzmann, S.; Riniker, S. Determining the Regiochemistry and Relative Stereochemistry of Small and Druglike Molecules Using an Alignment Algorithm for Infrared Spectra. *Anal. Chem.* **2020**, *92*, 9124–9131.

(S36) Jähnigen, S.; Zehnacker, A.; Vuilleumier, R. Computation of Solid-State Vibrational Circular Dichroism in the Periodic Gauge. *J. Phys. Chem. Lett.* **2021**, *12*, 7213–7220.

(S37) Frisch, M. J.; Pople, J. A.; Binkley, J. S. Self-consistent Molecular Orbital Methods 25. Supplementary Functions for Gaussian Basis Sets. *The Journal of Chemical Physics* **1984**, *80*, 3265–3269.

(S38) Grimme, S.; Ehrlich, S.; Goerigk, L. Effect of the Damping Function in Dispersion Corrected Density Functional Theory. *J. Comput. Chem.* **2011**, *32*, 1456–1465.

(S39) Halls, M. D.; Velkovski, J.; Schlegel, H. B. Harmonic Frequency Scaling Factors for Hartree-Fock, S-VWN, B-LYP, B3-LYP, B3-PW91 and MP2 with the Sadlej pVTZ Electric Property Basis Set. *Theor. Chem. Acc.* **2001**, *105*, 413–421.

(S40) Frisch, M. J.; Trucks, G. W.; Schlegel, H. B.; Scuseria, G. E.; Robb, M. A.; Cheeseman, J. R.; Scalmani, G.; Barone, V.; Petersson, G. A.; Nakatsuji, H.; Li, X.; Caricato, M.; Marenich, A.; Bloino, J.; Janesko, B. G.; Gomperts, R.; Mennucci, B.; Hratchian, H. P.; Ortiz, J. V.; Izmaylov, A. F.; Sonnenberg, J. L.; Williams-Young, D.; Ding, F.; Lipparini, F.; Egidi, F.; Goings, J.; Peng, B.; Petrone, A.; Henderson, T.; Ranasinghe, D.; Zakrzewski, V. G.; Gao, J.; Rega, N.; Zheng, G.; Liang, W.; Hada, M.; Ehara, M.; Toyota, K.; Fukuda, R.; Hasegawa, J.; Ishida, M.; Nakajima, T.; Honda, Y.; Kitao, O.; Nakai, H.; Vreven, T.; Throssell, K.; Montgomery, J. A.; Jr.,; Peralta, J. E.; Ogliaro, F.; Bearpark, M.; Heyd, J. J.; Brothers, E.; Kudin, K. N.; Staroverov, V. N.; Keith, T.; Kobayashi, R.; Normand, J.; Raghavachari, K.; Rendell, A.; Burant, J. C.; Iyengar, S. S.; Tomasi, J.; Cossi, M.; Millam, J. M.; Klene, M.; Adamo, C.; Cammi, R.; Ochterski, J. W.; Martin, R. L.; Morokuma, K.; Farkas, O.; Foresman, J. B.; Fox, D. J. Gaussian 16 Rev. B.01. Gaussian, Inc., Wallingford CT, 2016.

(S41) Hunter, J. D. Matplotlib: A 2D Graphics Environment. *Comput. Sci. Eng.* **2007**, *9*, 90–95.

(S42) Humphrey, W.; Dalke, A.; Schulten, K. VMD – Visual Molecular Dynamics. *J. Mol. Graph.* **1996**, *14*, 33–38.

(S43) Stone, J. Tachyon. An Efficient Library for Parallel Ray Tracing and Animation. 1995; `jedi.ks.uiuc.edu/~johns/raytracer`.

(S44) GIMP 2.8. `gimp.org`.